

Rf-induced persistent long-range ordered structures in two-species ion Coulomb crystals in a linear Paul trap.

A. Mortensen, E. Nielsen, T. Matthey, and M. Drewsen*

QUANTOP - Danish National Research Foundation Center for Quantum Optics,
Department of Physics and Astronomy, University of Aarhus, DK-8000 Aarhus C, Denmark

(Dated: August 23, 2006)

We report on the observations of persistent long-range ordered structures in the central $^{40}\text{Ca}^+$ ion component of $^{40}\text{Ca}^+ - ^{44}\text{Ca}^+$ two-species ion Coulomb crystals in a linear Paul trap. The lifetimes of structures consisting of a few thousand ions are several seconds, or at least an order of magnitude longer than observed in similar size single component systems [Phys. Rev. Lett. **96** 103001 (2006)]. Molecular dynamics simulations strongly indicate that the observed structures are induced by the radio frequency quadrupole trapping field.

PACS numbers: 32.80.Pj, 52.27.Jt, 52.27.Gr, 36.40.Ei

A solid state of an one-component plasma (OCP), often referred to as a Wigner crystal or a Coulomb crystal, appears whenever the coupling parameter $\Gamma = E_{\text{Coul}}/E_{\text{kin}}$, where E_{Coul} is the nearest neighboring Coulomb potential energy and E_{kin} is the averaged kinetic energy of the particles, exceeds ~ 200 [1, 2, 3]. In recent decades, such crystals have been investigated experimentally in a large variety of physical systems [4, 5, 6, 7]. In particular, laser-cooled and trapped atomic ions have proven to be an excellent system for experimental studies of Coulomb crystals under various confinement conditions. Single-species, one-, two- and three-dimensional ion Coulomb crystals have been investigated in Penning and radio frequency (rf) traps (also named Paul traps), with structural findings in good agreement with theoretical predictions [4, 8, 9, 10, 11, 12, 13]. Two-species crystals have been studied in much less detail, and experimentally mainly in linear Paul traps [13, 14]. For singly charged ions in such traps, the lighter species will in general segregate into a cylindrically shaped structure surrounded by the heavier ion species. In the case of $^{40}\text{Ca}^+$ and $^{24}\text{Mg}^+$ ions, the structures of the lighter species [13] were found for the most part to be identical to the cylindrical structures of infinitely long one-species systems confined in two-dimensions by a rotational-symmetric harmonic potential [15]. For two ion species with identical charge-to-mass ratios, mixing of the species is predicted [16]. At present, Coulomb crystals find applications in such diverse fields as quantum computing [17, 18] and cold molecule ion research [14, 19, 20].

In this Letter, we present observations of persistent long-range ordered structures in the $^{40}\text{Ca}^+$ component of bicrystals consisting of $^{40}\text{Ca}^+$ and $^{44}\text{Ca}^+$ ions. The observed structures deviate from those expected for a fully rotational symmetric harmonic potential [13, 15], but are in close agreement with results from molecular dynamics (MD) simulations including the quadrupole nature of the trapping fields.

The Ca^+ ions are confined in a linear Paul trap which is situated in a vacuum chamber at a pressure of 10^{-10} Torr,

and are laser cooled as depicted in Fig. 1(a). The Paul trap used in these experiments has been described in detail elsewhere [21]. In short, the linear Paul trap consists of four electrode rods placed in a quadrupole configuration. The electrode diameter is 8.0 mm and the minimum distance of the central trap axis is $r_0 = 3.5$ mm. Time varying voltages $\frac{1}{2}U_{\text{rf}} \cos(\Omega_{\text{rf}}t)$ and $\frac{1}{2}U_{\text{rf}} \cos(\Omega_{\text{rf}}t + \pi)$ are applied to the two sets of diagonally opposite electrode rods, respectively, to obtain confinement in the radial plane (xy -plane in Fig. 1(a)). Axial confinement along the z -axis is accomplished by sectioning each of the electrode rods into three pieces and then applying a static voltage U_{end} to the end-electrodes. The length of the center-electrode is 5.4 mm, while the outer pieces are 20 mm. In the present experiments $\Omega_{\text{rf}} = 2\pi \times 3.88$ MHz, $U_{\text{rf}} \sim 540$ V and $U_{\text{end}} \sim 10$ –50 V were used. The resulting confinement for an ion species of type i with mass M_i and charge Q_i is well described by a harmonic pseudo potential $\Phi_{\text{ps}}(r, z) = \frac{1}{2}M_i(\omega_r^2 r^2 + \omega_z^2 z^2)$, where ω_r and ω_z are the radial and axial trap frequencies, respectively. The axial trap frequency is given by $\omega_z^2 = 2\kappa Q_i U_{\text{end}}/M_i$, where $\kappa = 3.97 \times 10^4 \text{ m}^{-2}$ is a constant related to trap geometry, and the radial trap frequency is given by $\omega_r^2 = \omega_{\text{rf}}^2 - \frac{1}{2}\omega_z^2$, where $\omega_{\text{rf}}^2 = Q_i^2 U_{\text{rf}}^2 / 2M_i r_0^4 \Omega_{\text{rf}}^2$ is the contribution from the time varying trapping fields. The dependence on the charge and mass of the ion species makes the lighter isotope ($^{40}\text{Ca}^+$) more tightly bound towards the trap axis than the heavier ($^{44}\text{Ca}^+$) and leads consequently to a total radial separation of the two ion species when sufficiently cooled [13]. The zero-temperature ion density in the pseudopotential is given by $n_{\text{theo}} = \epsilon_0 U_{\text{rf}}^2 / M_i r_0^4 \Omega_{\text{rf}}^2$, where ϵ_0 is the vacuum permittivity [13]. Due to the spatial separation of the ions in two-species ion Coulomb crystals, this expression is also applicable to the individual components of such crystals.

The $^{40}\text{Ca}^+$ and $^{44}\text{Ca}^+$ ions used in the experiments are produced isotope selectively by resonant two-photon photo-ionization of atoms in an effusive beam of naturally abundant calcium [22, 23]. In Fig. 1(b), the transitions in Ca^+ used for Doppler laser cooling of the trapped ions

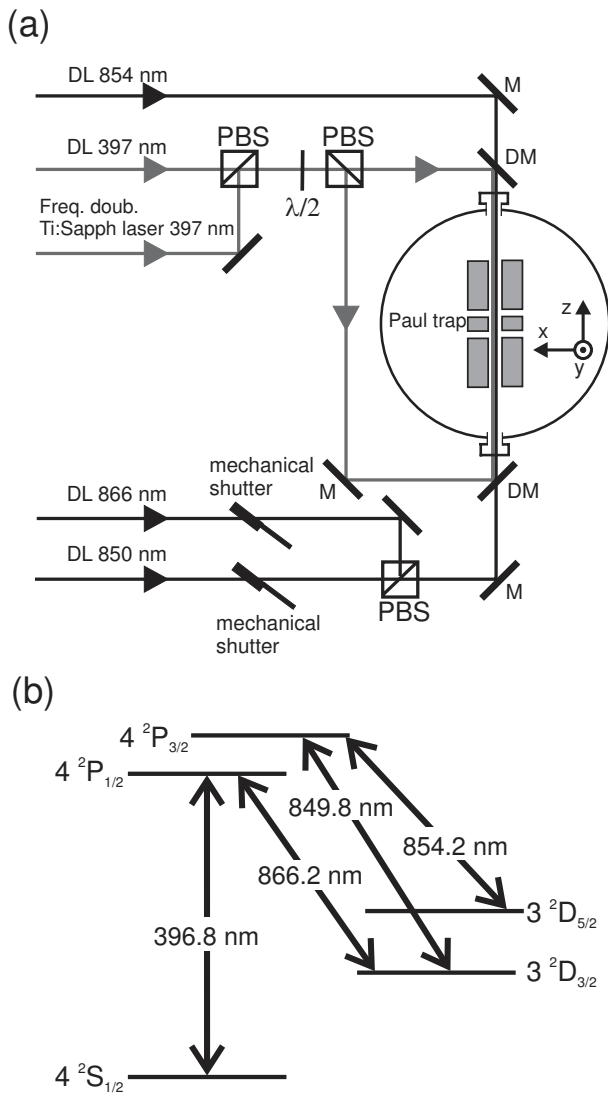


FIG. 1: (a) Schematics of the laser and linear Paul trap setup. (D)M denotes a (dichroic) mirror, PBS denotes polarization beamsplitters, and DL denotes diode laser. (b) Optical transitions used for Doppler laser cooling of the Ca^+ ions.

are shown. The main cooling transition is the dipole allowed $4S_{1/2} \rightarrow 4P_{1/2}$ transition at 397 nm. To avoid optical pumping into the metastable $3D_{3/2}$ state, repumping is done either by using a single repump laser at 866 nm via the $4P_{1/2}$ state ($^{44}\text{Ca}^+$) or by using two repump lasers at 850 nm and 854 nm via the $4P_{3/2}$ state ($^{40}\text{Ca}^+$). Due to the isotope shifts of the cooling transitions [24, 25], each isotope ion requires its own laser cooling frequencies. As indicated in Fig. 1(a), we use a 397 nm frequency doubled Ti:Sapphire laser and a 866 nm diode laser for the cooling of $^{44}\text{Ca}^+$ ions, while for the $^{40}\text{Ca}^+$ ions 850 nm and 854 nm diode lasers are applied. For both isotopes the final temperature is of the order of ~ 10 mK, which is low enough for achieving Coulomb crystallization ($\Gamma \sim 250$ [2]). Imaging of the fluorescence from the

trapped ions is achieved using an image intensified CCD camera placed above the trap.

Images of two-species Coulomb crystals consisting of $^{40}\text{Ca}^+$ and $^{44}\text{Ca}^+$ ions are presented in Fig. 2 for various settings of the static voltage U_{end} on the end-electrodes. Since the ions are only fluorescing when they are directly laser cooled, the two isotopes can be imaged separately by alternately blocking (about 1 Hz rep. rate) the 850 nm ($^{40}\text{Ca}^+$ laser cooling off) and the 866 nm laser ($^{44}\text{Ca}^+$ laser cooling off) using mechanical shutters. The presented combined images are subsequently created with a red color coding for $^{40}\text{Ca}^+$ and blue for $^{44}\text{Ca}^+$. Due to sympathetic cooling [26, 27], the crystal retains its shape and structure during the alternating laser cooling sequence. As expected [13], the lightest isotope $^{40}\text{Ca}^+$ is located as a cylindrical core closest to the trap axis, surrounded by the heavier $^{44}\text{Ca}^+$. It is immediately clear from the images in Fig. 2 that the projection of the actual three-dimensional structure of the $^{40}\text{Ca}^+$ ions is a two-dimensional rectangular lattice aligned with the trap axis. Since the depth of focus of the imaging system ($\sim 50 \mu\text{m}$) is several times the inter-ion distance, we conclude the rectangular structure in the images must originate from a three-dimensional long-range ordering [8]. In contrast to our previous observations of long-range order in spherical one-component ion crystals [8], where the orientation of the observed metastable (~ 100 ms) structures seemed to be arbitrary, the rectangular structures presented here are very persistent (~ 10 s) and always oriented the same way. Accordingly, we conclude that the presence of the surrounding $^{44}\text{Ca}^+$ ions has a great impact on the formation and appearance of the observed long-range structure in the $^{40}\text{Ca}^+$ part of the crystal. The image sequence in Fig. 2 illustrates additionally that despite changes in the outer shape of the $^{40}\text{Ca}^+$ core, the observed rectangular lattice of the ions is preserved, indicating that the observed long-range ordered structure is rather stable to changes in the boundary conditions of the crystal.

In order to understand the observations, a series of molecular dynamics (MD) simulations of two-species crystals with the same number of the two calcium isotope ions as in the crystals shown in Fig. 2 have been performed. In Figs. 3(a) and 3(b), results from one simulation using a pseudo-potential corresponding to the trapping parameters of Fig. 2(b) is presented. As in the experiments, a clear radial separation of the two isotope ions is observed. Furthermore the radial projection (Fig. 3(a)) clearly reveals that the $^{40}\text{Ca}^+$ part of the crystal is organized in concentric cylindrical structures, resembling the structure of an infinitely long 1D cylindrically symmetric confined ion crystal [13, 15]. In Fig. 3(b), a projection corresponding to the focal region of the imaging system is shown. Neither this nor other sections, e.g., in the yz -plane, lead to projection images with rectangular structures. However, when the

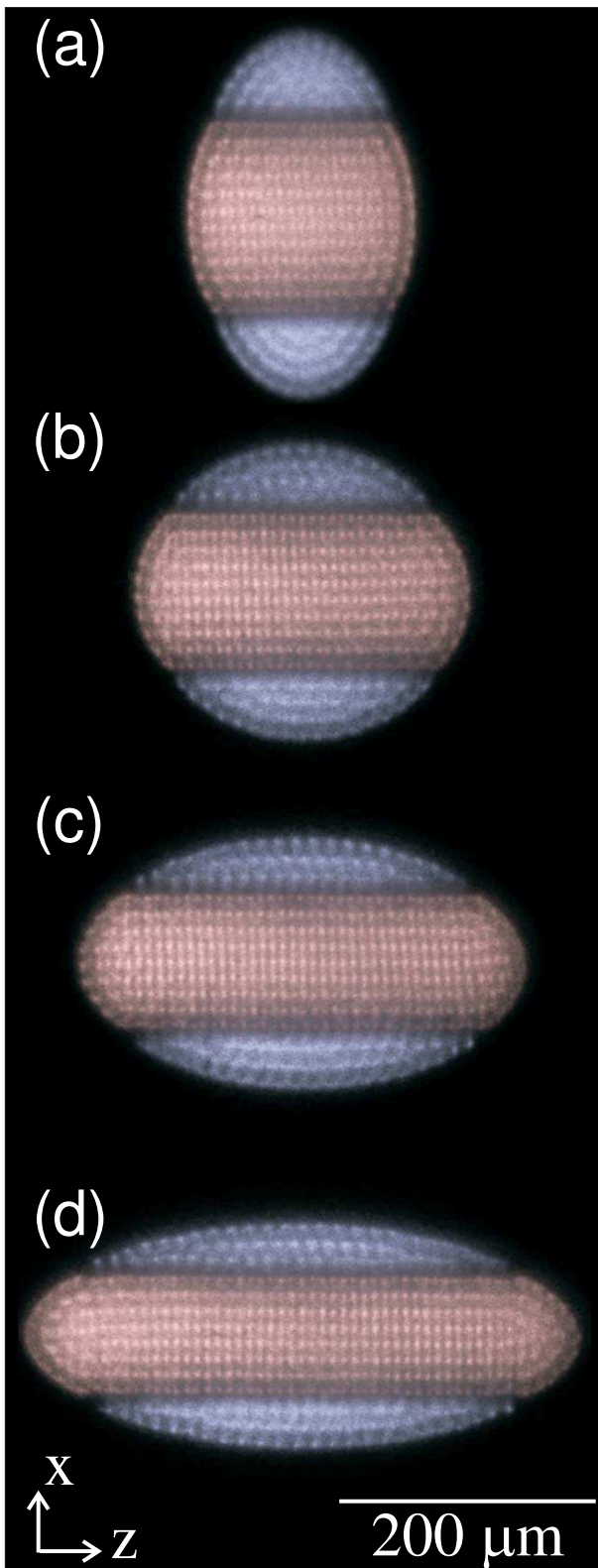


FIG. 2: (color online) Images of two-species ion Coulomb crystals containing ~ 1500 $^{40}\text{Ca}^+$ ions (red) and ~ 2000 $^{44}\text{Ca}^+$ ions (blue) at different settings of the end-cap potential, U_{end} . The camera exposure time is ~ 100 ms and the trap potentials are $U_{\text{rf}} = 540$ V and (a) $U_{\text{end}} = 46.1$ V, (b) $U_{\text{end}} = 30.2$ V, (c) $U_{\text{end}} = 20.0$ V, and (d) $U_{\text{end}} = 13.8$ V, respectively.

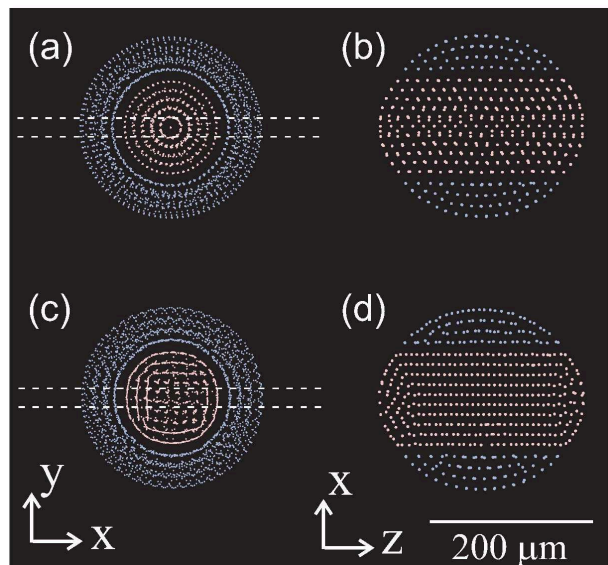


FIG. 3: (color online) MD simulation data of a two-species ion Coulomb crystal containing 1500 $^{40}\text{Ca}^+$ ions (red) and 2000 $^{44}\text{Ca}^+$ ions (blue) using a pseudo potential approximation ((a) and (b)) and using the full rf potential ((c) and (d)), respectively. While (a) and (c) show a projection of all the ion positions onto the xy -plane, (b) and (d) present the data points contained in a slice of thickness $24 \mu\text{m}$ through the crystal center projected to the xz -plane. The slices are indicated by white dashed lines in (a) and (c). Trap potentials are $U_{\text{rf}} = 540$ V and $U_{\text{end}} = 33$ V.

full rf potential is used in the MD simulations, some regular ordering in the central component of the crystal does appear, as is evident from the results presented in Figs. 3(c) and 3(d) for a specific phase of the rf field. From Fig. 3(d), it is seen that indeed a rectangular projection image is expected when the rf-quadrupole field, which breaks the rotational symmetry, is included in the simulations. Even when averaging over all phases of the rf field, the rectangular structure persists. However, some blurring of the position of the ions along the x -axis, as is seen in the images of Fig. 2, is found. Analysis of a much simpler two-ion system in a linear rf trap has previously shown similar preferred orientation effects with respect to the rf quadrupole field axes [28].

A closer analysis of the simulation results presented in Figs. 3(c) and 3(d) shows that the $^{40}\text{Ca}^+$ ions in the core organize themselves in a long-range ordered structure in the form of a face-centered tetragonal (fct) lattice as illustrated in Fig. 4(a), with the sidelengths related by $a = b = c/\sqrt{3}$. The rectangular projection presented in Fig. 3(d) is obtained when the fct structure is viewed along the b vector as illustrated in Fig. 4(b). This rectangular projection has a height to width ratio of $h_{\text{fct}}/w_{\text{fct}} \simeq 1.73$, which is not exactly the same as the $h/w = 1.62 \pm 0.07$ observed in the experiments. In fact, the observed rectangular structure is more in agreement

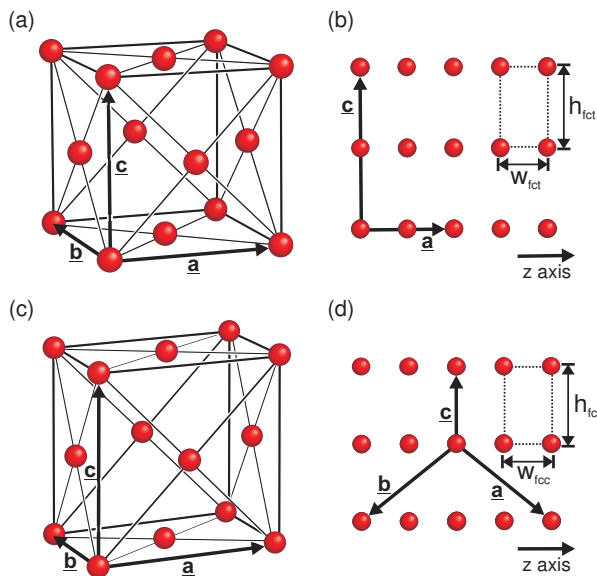


FIG. 4: Fct (a) and fcc (b) lattice cells. (c) Projection along the [211]-direction of the fcc lattice and (d) projection along the b vector of the fct lattice.

with a face-centered cubic (fcc) structure viewed along the [211] direction (see Figs. 4(c) and 4(d)), which would lead to $h_{fcc}/w_{fcc} \simeq 1.63$. The reason for the deviation between the simulated results and the actually observed structures is probably that the difference in the potential energies of the two structures in the rf potential is very small, as is well-known to be the case for various long-range ordered structures in infinite systems without the presence of rf fields [3]. In recent single component experiments both body-centered cubic (bcc) and fcc-like structures were indeed observed [8], but in contrast to the two-species results above, no fixed orientation with respect to the trap axis was found. Another point supporting that the observed structure is a fcc structure is the ion density. Assuming that the observed projection images of $^{40}\text{Ca}^+$ ions in Fig. 2 are actually fcc structures observed along the [211] direction, the ion density must be $n_{fcc} = (3.8 \pm 0.4) \times 10^8 \text{ cm}^{-3}$. In comparison, the $^{40}\text{Ca}^+$ ion density calculated from the trap parameters is $n_{\text{theo},40} = (4.3 \pm 0.3) \times 10^8$, in good agreement with the fcc assumption.

In conclusion, very persistent three-dimensional long-range ordered structures have been observed in $^{40}\text{Ca}^+$ - $^{44}\text{Ca}^+$ two-species ion Coulomb crystals in a linear Paul trap. The observed structures and their orientations are found to be in reasonable agreement with MD results only when the rf quadrupole field is included in the simulations. Very stable oriented crystal structures such as these may in the future find many applications as, for example, atomic media for cavity QED studies and quantum memories for light [29].

We acknowledge financial support from the Carlsberg

Foundation as well as from the Danish National Research Foundation: Center for Quantum Optics, QUANTOP.

* E-mail: drewsen@phys.au.dk

- [1] E. L. Pollock and J. P. Hansen, *Phys. Rev. A* **8**, 3110 (1973).
- [2] J. P. Schiffer, *Phys. Rev. Lett.* **88**, 205003 (2002).
- [3] D. H. E. Dubin, *Phys. Rev. A* **40**, 1140 (1989).
- [4] G. Birkl, S. Kassner, and H. Walther, *Nature* **357**, 310 (1992).
- [5] C. C. Grimes and G. Adams, *Phys. Rev. Lett.* **42**, 795 (1979).
- [6] E. Y. Andrei, G. Deville, D. C. Glattli, F. I. B. Williams, E. Paris, and B. Etienne, *Phys. Rev. Lett.* **60**, 2765 (1988).
- [7] H. Thomas, G. E. Morfill, V. Demmel, J. Goree, B. Feuerbacher, and D. Möhlmann, *Phys. Rev. Lett.* **73**, 652 (1994).
- [8] A. Mortensen, E. Nielsen, T. Matthey, and M. Drewsen, *Phys. Rev. Lett.* **96**, 103001 (2006).
- [9] M. Drewsen, C. Brodersen, L. Hornekær, J. S. Hangst, and J. P. Schiffer, *Phys. Rev. Lett.* **81**, 2878 (1998).
- [10] T. Schätz, U. Schramm, and D. Habs, *Nature* **412**, 717 (2001).
- [11] T. B. Mitchell, J. J. Bollinger, D. H. E. Dubin, X.-P. Huang, W. M. Itano, and R. H. Baughman, *Science* **282**, 1290 (1998).
- [12] W. M. Itano, J. J. Bollinger, J. N. Tan, B. Jelenković, X.-P. Huang, and D. J. Wineland, *Science* **279**, 686 (1998).
- [13] L. Hornekær, N. Kjærgaard, A. M. Thommesen, and M. Drewsen, *Phys. Rev. Lett.* **86**, 1994 (2001).
- [14] P. Blythe, B. Roth, U. Frohlich, H. Wenz, and S. Schiller, *Phys. Rev. Lett.* **95**, 183002 (2005).
- [15] R. W. Hasse and J. P. Schiffer, *Ann. Phys.* **203**, 419 (1990).
- [16] T. Matthey, J. P. Hansen, and M. Drewsen, *Phys. Rev. Lett.* **91**, 165001 (2003).
- [17] M. Riebe, H. Häffner, C. F. Roos, W. Hänsel, J. Benhelm, G. P. T. Lancaster, T. W. Körber, C. Becher, F. Schmidt-Kaler, D. F. V. James, et al., *Nature* **429**, 734 (2004).
- [18] M. D. Barrett, J. Chiaverini, T. Schaetz, J. Britton, W. M. Itano, J. D. Jost, E. Knill, C. Langer, C. Leibfried, R. Ozeri, et al., *Nature* **429**, 737 (2004).
- [19] K. Møllhave and M. Drewsen, *Phys. Rev. A* **62**, 011401(R) (2000).
- [20] A. Bertelsen, S. Jørgensen, and M. Drewsen, *Journal of Physics B: Atomic, Molecular and Optical Physics* **39**, L83 (2006).
- [21] M. Drewsen, I. Jensen, J. Lindballe, N. Nissen, R. Martinussen, A. Mortensen, P. Staantum, and D. Voigt, *Int. J. Mass Spectrom.* **229**, 83 (2003).
- [22] N. Kjærgaard, L. Hornekær, A. Thommesen, Z. Videsen, and M. Drewsen, *Appl. Phys. B* **71**, 207 (2000).
- [23] A. Mortensen, J. J. T. Lindballe, I. S. Jensen, P. Staantum, D. Voigt, and M. Drewsen, *Phys. Rev. A* **69**, 042502 (2004).
- [24] A.-M. Mårtensson-Pendrill, A. Ynnerman, H. Warston, L. Vermeeren, R. E. Silverans, A. Klein, R. Neugart, C. Schulz, P. Lievens, and The ISOLDE Collaboration, *Phys. Rev. A* **45**, 4675 (1992).

- [25] W. Alt, M. Block, V. Schmidt, T. Nakamura, P. Seibert, X. Chu, and G. Werth, *J. Phys. B* **30**, L677 (1997).
- [26] D. J. Larson, J. C. Bergquist, J. J. Bollinger, W. M. Itano, and D. J. Wineland, *Phys. Rev. Lett.* **57**, 70 (1986).
- [27] P. Bowe, L. Hornekær, C. Brodersen, M. Drewsen, J. S. Hangst, and J. P. Schiffer, *Phys. Rev. Lett.* **82**, 2071 (1999).
- [28] M. Drewsen and A. Brøner, *Phys. Rev. A* **62**, 045401 (2000).
- [29] A. Mortensen, Ph.D. thesis, University of Aarhus (2005).